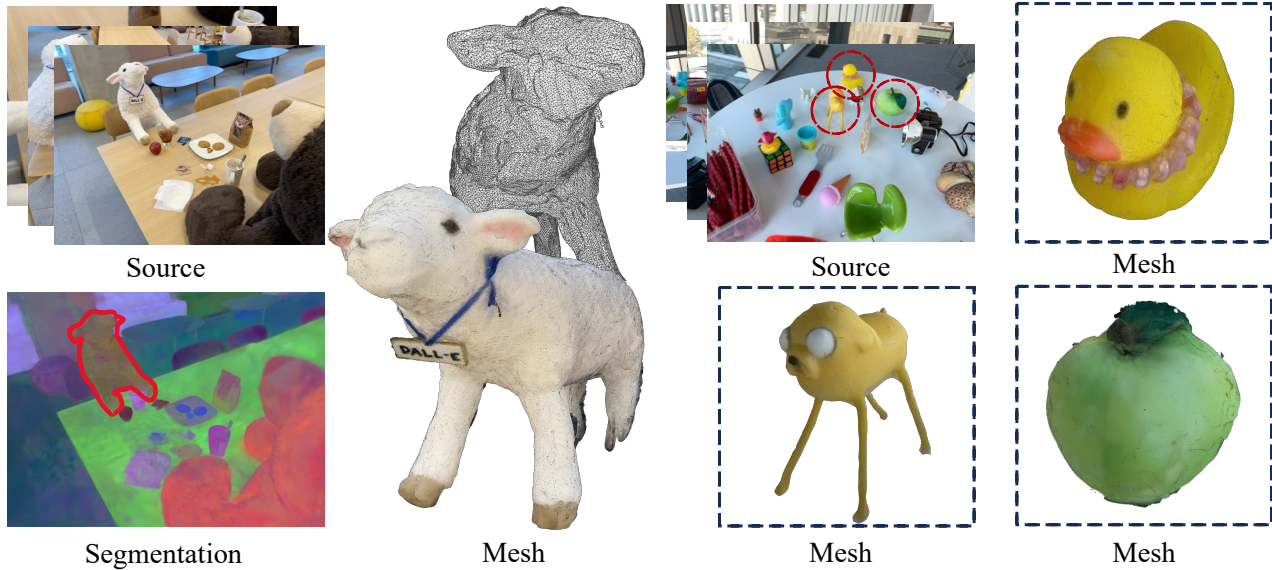


# OMEGAS: Object Mesh Extraction from Large Scenes Guided by Gaussian Segmentation

Lizhi Wang\*, Feng Zhou\*, Jianqin Yin†  
 Beijing University of Posts and Telecommunications  
 wanglizhi@bupt.edu.cn



**Figure 1:** Our OMEGAS segments and generates high-quality meshes for specified objects in open-world scenes, enabling the acquisition of higher quality meshes while reducing editing workload, thus suitable for downstream tasks such as AR, gaming, and large-scale 3D dataset generation.

## ABSTRACT

Recent advancements in 3D reconstruction technologies have paved the way for high-quality and real-time rendering of complex 3D scenes. Despite these achievements, a notable challenge persists: it is difficult to precisely reconstruct specific objects from large scenes. Current scene reconstruction techniques frequently result in the loss of object detail textures and are unable to reconstruct object portions that are occluded or unseen in views. To address this challenge, we delve into the meticulous 3D reconstruction of specific objects within large scenes and propose a framework termed **OMEGAS: Object Mesh Extraction from Large Scenes Guided by GAussian Segmentation**. OMEGAS employs a multi-step approach, grounded in several excellent off-the-shelf methodologies. Specifically, initially, we utilize the Segment Anything Model (SAM) to

guide the segmentation of 3D Gaussian Splatting (3DGS), thereby creating a basic 3DGS model of the target object. Then, we leverage large-scale diffusion priors to further refine the details of the 3DGS model, especially aimed at addressing invisible or occluded object portions from the original scene views. Subsequently, by re-rendering the 3DGS model onto the scene views, we achieve accurate object segmentation and effectively remove the background. Finally, these target-only images are used to improve the 3DGS model further and extract the definitive 3D object mesh by the SuGaR model. In various scenarios, our experiments demonstrate that OMEGAS significantly surpasses existing scene reconstruction methods.

## CCS CONCEPTS

• Computing methodologies → Reconstruction.

## KEYWORDS

Mesh Reconstruction, 3D Gaussian Splatting, Diffusion Model

Permission to make digital or hard copies of all or part of this work for personal or classroom use is granted without fee provided that copies are not made or distributed for profit or commercial advantage and that copies bear this notice and the full citation on the first page. Copyrights for components of this work owned by others than ACM must be honored. Abstracting with credit is permitted. To copy otherwise, or republish, to post on servers or to redistribute to lists, requires prior specific permission and/or a fee. Request permissions from [permissions@acm.org](mailto:permissions@acm.org).

MM '24, October 28–November 1, 2024, Melbourne, Australia

© 2024 Association for Computing Machinery.  
 ACM ISBN 978-x-xxxx-xxxx-x/YY/MM... \$15.00  
<https://doi.org/XXXXXXXX.XXXXXXX>

\*Contributed equally.

†Corresponding author.



**Figure 2: Comparing the reconstruction effects of the occluded or unseen portions of the object, OMEGAS demonstrates effective capabilities in reconstructing invisible parts of objects.**

## 1 INTRODUCTION

In recent years, the field of 3D reconstruction has emerged as a pivotal area of research, driven by its profound applications across a diverse range of disciplines, including robotics [30], architectural design [3], virtual reality [37], and so on. The community has achieved high-quality and real-time complex 3D scene reconstruction and rendering thanks to the development of 3D rendering-based reconstruction models, *i.e.*, neural radiation field (NeRF) -based models [1, 2, 24, 43] and 3D Gaussian Splatting (3DGS) -based models [15, 22, 36, 40].

However, existing methods struggle to reconstruct a target object’s 3D mesh given scene images, which is somehow more solid and straightforward in downstream applications like virtual game modeling. For one thing, the reconstruction of entire scenes often leads to a compromise in the quality of specific object reconstruction. Furthermore, certain parts of a specific object in a scene are frequently occluded or invisible from any perspective, making their reconstruction challenging with current methods, as illustrated in Figure 2.

To address this challenge, we propose a novel and effective framework that reconstructs the 3D mesh of the target object given multi-view open-world scene images, termed OMEGAS: Object Mesh Extraction from Large Scenes Guided by Gaussian Segmentation. As shown in Figure 1, given the multi-view scene images, our framework can freely select and segment the target object from images and extract accurate 3D object mesh. Our framework is built on several excellent off-the-shelf methods to achieve high-precision extraction in a multi-step way.

Inspired by Gaussian Grouping [41], we first leverage the Segment Anything Model (SAM) [18] and 3D Gaussian Splatting (3DGS) [15] to segment the 3D consistency mask of the target object in multi-view images and construct a base target 3DGS model. Specifically, we add a compact identity vector of length 8 for each Gaussian, enabling the segmentation of multiple objects. Subsequently, we

extract the 2D rendered identity vectors and apply an additional linear layer to classify these projected embeddings with cross-entropy loss. To further boost the segmentation accuracy of Gaussians, we also introduce an unsupervised 3D cosine similarity loss. Our experiments demonstrate that this can improve segmentation accuracy while also enhancing efficiency. We adopt Grounding DINO [21] to select the object and then extract the Gaussians.

Subsequently, in addressing the occluded portions of the target and enhancing the texture detail, we utilize large-scale diffusion priors (*i.e.*, Stable Diffusion) to optimize the 3DGS model of the target through random camera rendering. We utilize the Score Distillation Sampling (SDS) loss [27] with the prompt of “a photo of the object”.

Ultimately, by re-rendering the 3DGS model onto the input images, we are able to derive more precise target masks from multiple views. This process enables us to obtain images of the target object devoid of background. Since the original scene images do not include any occluded or unseen parts of the object, which can impair the effectiveness of the SuGaR model, we enhance these object-only images by randomly rendering the target 3D Gaussian shape (3DGS) model. Further, by amalgamating these images with the refined target 3DGS model, we utilize the SuGaR [11] model to execute the final optimization of the 3DGS and to extract the ultimate mesh.

Extensive experiments demonstrate the superior performance of our framework, capable of reconstructing the target object mesh with high precision. Besides, visualization experiments show that our method also has a good reconstruction effect on the obscured or invisible parts of the target.

In summary, our contributions are:

- We propose OMEGAS, an effective framework to extract meshes of specified objects through multi-view 2D images in open-world scenes.
- We ingeniously integrate several off-the-shelf generative approaches: SAM is leveraged to guide the segmentation of

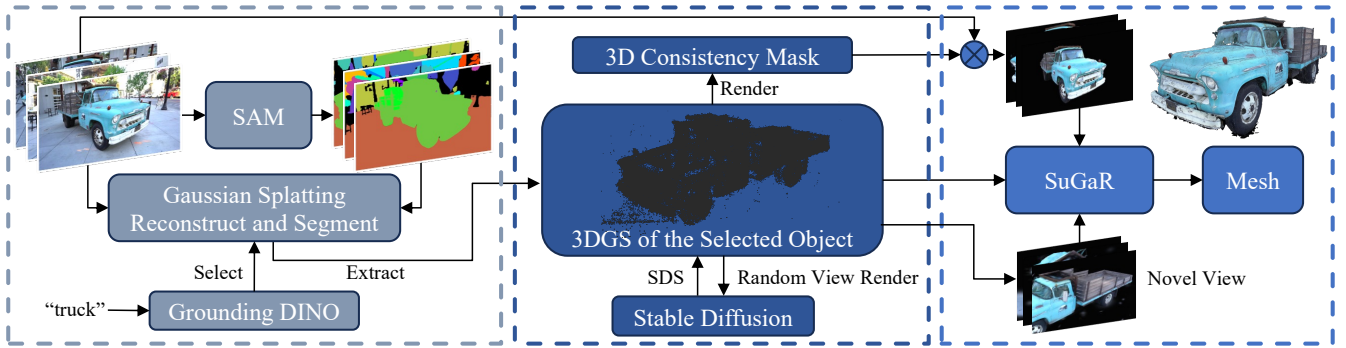


**Figure 3: The pipeline of OMEGAS.** We use object-oriented 3D Gaussians to represent the scene, segment all objects using IDs generated by SAM, extract target object 3DGS by the guidance of Grounding DINO, iterate optimization using Stable Diffusion by SDS loss, and finally extract meshes using SuGaR.

the target 3DGS model; large diffusion priors are utilized to enhance details and the occluded parts of the 3DGS model; finally, SuGaR is employed for further refinement and extraction of the final target mesh.

- Extensive experiments reveal that OMEGAS operates effectively in a range of open-world scenes and significantly surpasses the existing approach in performance. Specifically, our approach shows superiority in both texture details and occlusion robustness on target object reconstruction.

## 2 RELATED WORKS

### 2.1 Segmentation of Rendering-based 3D Models

Due to the intrinsic implicit nature of the rendering-based model, it’s hard to do normal data-driven training for semantic segmentation like explicit 3D models (e.g., 3D point-cloud segmentation [9, 38]). To address this issue, Spin-NeRF [9] first proposes a method that segments specific objects in NeRF and achieves inpainting in different views with 3D consistency. Recently, 3D Gaussian Splatting established its effectiveness in the reconstruction task exhibiting high inference speeds and remarkable quality. Following Spin-NeRF, Gaussian Grouping [41] extends the object-oriented concept from Spin-NeRF to 3D Gaussian Splatting, enabling the joint reconstruction and segmentation of anything in open-world 3D scenes and various 3D editing tasks. Different from Gaussian Grouping, our framework is tailored specifically for the segmentation of particular objects in 3DGS within large scenes, with the goal of achieving precise object reconstruction in expansive scenes.

### 2.2 Mesh Extraction from Images

In the early days, the development of Structure-from-motion (SfM) [31] and Multi-View Stereo (MVS) [10] allows for 3D reconstruction from multi-view images. More recently, owing to the development of neural network-based 3D reconstruction method [15, 24], various approaches have explored integrating rendering-based models with mesh reconstruction. [8, 20, 26, 34, 39] For example, some works optimize neural signed distance functions (SDF) by training neural radiance fields (NeRF) in which the density is derived

as a differentiable transformation of the SDF [20, 26]. A triangle mesh can finally be reconstructed from the SDF by applying the Marching Cubes algorithm[23]. Notably, SuGaR [11] introduced the pioneering method for high-precision mesh reconstruction from a 3DGS model. Our research builds upon SuGaR to extract the final object mesh.

### 2.3 3D Optimization by Diffusion Priors

Recently, with advancements in large-scale open-world diffusion generative models [5], certain studies have utilized diffusion priors to facilitate text/image-to-3D tasks. DreamFusion [27] introduces a technique known as Score Distillation Sampling (SDS), also referred to as Score Jacobian Chaining [33], to create object NeRFs from text prompts. GCFG [4] presents a guidance-decoupled personalization framework for customizing large-scale diffusion priors for specific concepts as concept-centric personalization. ProlificDreamer [35] extends SDS to Variational Score Distillation (VSD) for high-fidelity and diverse text-to-3D Generation. After the emerging of 3D Gaussian Splatting, some approaches [32, 42] develop a pipeline for producing high-quality object meshes from text or image inputs with 3DGS models. In our framework, we employ SDS loss to effectively address the unseen or occluded portions of the target object.

## 3 METHOD

Our framework aims to reconstruct the mesh of the target object given multi-view scene images. Our work is built on or draws inspiration from several excellent off-the-shelf approaches, including Segment Anything Model (SAM) [6], Gaussian Grouping [41], Stable Diffusion [28], and SuGaR [11]. In essence, following the Gaussian Grouping, our initial step involves leveraging SAM to guide the segmentation of 3DGS, extracting in a basic target 3DGS model. Subsequently, we apply large-scale open-world diffusion priors (i.e., Stable Diffusion) to enhance the model’s details and address its unseen parts. Next, we re-render the 3DGS onto the scene image to obtain accurate object masks and eliminate the background. Ultimately, the isolated images of the object and the 3DGS model are integrated into the SuGaR Model for further refinement and the

extraction of the object mesh; the overall framework is shown in Figure 3.

The rest of this section is organized as follows: in Sec 3.1, we first briefly review the 3D Gaussian Splatting method, diffusion prior guidance, and the SuGaR model; in Sec 3.2, we introduce our Gaussian segmentation pipeline in detail; In Sec 3.3, we introduce the 3DGS optimization process by Stable Diffusion; In Sec 3.4: we introduce the final mesh extraction process.

### 3.1 Preliminaries

**3D Gaussian Splatting (3DGS)** [15] provides an effective representation for novel-view synthesis and 3D reconstruction. Different from those implicit counterparts like NeRF [24], 3D Gaussian Splatting represents the underlying scene using a collection of anisotropic Gaussians. These Gaussians are parameterized by their center position  $\mu \in \mathbb{R}^3$ , covariance  $\Sigma \in \mathbb{R}^7$ , color  $c \in \mathbb{R}^3$ , and opacity  $\alpha \in \mathbb{R}$ . By projecting 3D Gaussians onto the camera’s imaging plane, the 2D Gaussians are assigned to the corresponding tiles for point-based rendering:

$$G(p, \mu_i, \Sigma_i) = \exp\left(-\frac{1}{2}(p - \mu_i)^\top \Sigma_i^{-1}(p - \mu_i)\right),$$

$$c(p) = \sum_{i \in \mathcal{N}} c_i \sigma_i \prod_{j=1}^{i-1} (1 - \sigma_j), \quad \sigma_i = \alpha_i G(p, \mu_i, \Sigma_i), \quad (1)$$

where  $p$  is the location of queried point;  $\mu_i, \Sigma_i, c_i, \alpha_i$ , and  $\sigma_i$  are the center position, covariance, color, opacity, and density of the  $i$ -th Gaussian, respectively;  $G(p, \mu_i, \Sigma_i)$  is the value of the  $i$ -th Gaussian at point  $p$ ;  $\mathcal{N}$  denotes the set of 3D Gaussians in this tile. Furthermore, 3D Gaussian Splatting enhances a GPU-optimized rasterization process, resulting in superior quality, accelerated rendering speed, and reduced memory consumption.

**Score Distillation Sampling (SDS)** is proposed in DreamFusion [27] to distill the 2D pre-trained diffusion prior for optimizing 3D representations. Specifically, we represent a 3D scene parameterized by  $\theta$  and use a differentiable rendering function  $g(\cdot)$  to obtain an image  $\mathbf{x} = g(\theta)$ . By pushing samples towards denser regions of the real-data distribution across all noise levels, we make renderings from each camera view resemble the plausible samples derived from the guidance diffusion model  $\phi$ . In practice, DreamFusion uses Imagen [29] as the score estimation function  $\epsilon_\phi(\mathbf{x}_t; y)$ , which predicts the sampled noise  $\epsilon_\phi$  given the noisy image  $\mathbf{x}_t$ , text embedding  $y$ , and timestep  $t$ . SDS optimizes 3D scenes using gradient descent with respect to  $\theta$ :

$$\nabla_\theta \mathcal{L}_{\text{SDS}} = \mathbb{E}_{\epsilon, t} \left[ w_t \left( \epsilon_\phi(\mathbf{x}_t; y) - \epsilon \right) \frac{\partial \mathbf{x}}{\partial \theta} \right], \quad (2)$$

where  $\epsilon \sim \mathcal{N}(0, \mathbf{I})$  is a Gaussian noise;  $\mathbf{x}_t = \alpha_t \mathbf{x} + \sigma_t \epsilon$  is the noised image;  $\alpha_t, \sigma_t$ , and  $w_t$  are noise sampler terms.

**SuGaR** [11] proposes an accurate and extremely fast method for extracting meshes from 3D Gaussian Splatting. It proposes a regularization term that makes the Gaussians capture accurately the geometry of the scene. The term  $\mathcal{R}$  can be formulated as:

$$\mathcal{R} = \frac{1}{|\mathcal{P}|} \sum_{p \in \mathcal{P}} |\hat{f}(p) - f(p)|, \quad (3)$$

where  $p$  is the sampled 3D points,  $f(p)$  refers to the ideal SDF, and  $\hat{f}(p)$  represents the estimated SDF of the surface created by the current Gaussians.  $\mathcal{P}$  refers to the set of sampled points.

SuGaR runs a Poisson Reconstruction [13] on the sampled 3D points on a level set of the density computed from the Gaussians to create a mesh from Gaussians obtained after optimization using the regularization term. After extracted the first mesh, SuGaR refines this mesh by binding new Gaussians to the mesh triangles and optimizing the Gaussians and the mesh jointly using the Gaussian Splatting rasterizer.

### 3.2 Gaussian Segmentation

**Scene Segmentation by SAM.** We first conduct preliminary target consistency segmentation on scene images from different views based on SAM’s capabilities in open-world segmentation for intricate scenes. Specifically, following [41], we treat scene images from divergent views as a continuous video sequence and feed them to SAM for initial segmentation. Then, we apply Track anything [7] on those segmentation results. This process enables us to assign unique object IDs, ranging from 0 to 255. The segmented outcomes are preserved as gray-scale images, with each object’s ID represented in corresponding gray-scale values.

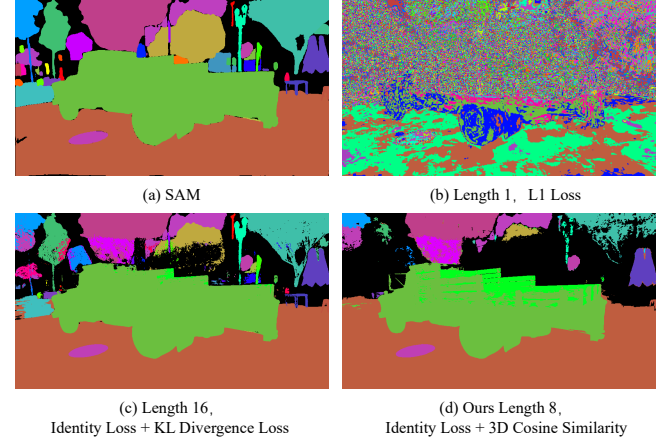


**Figure 4: Comparing the segmentation effects of different vector lengths and loss functions on the truck scene from Tanks&Temples dataset[19].** Figure (a) shows the initial segmentation generated by SAM; Figure (b) presents segmentation via 3D Gaussian Splatting for grayscale scene reconstruction. Figure (c) employs Gaussian grouping for segmentation, whereas Figure (d) utilizes our method. The imprecision of SAM leads to poor fitting in Figure (a), a challenge our method overcomes. Moreover, our segmentation technique exhibits enhanced precision when compared to Gaussian Grouping, which we have quantified in Table 1.

**3DGS Reconstruction and Segmentation.** We leverage the grayscale images to guide the segmentation of 3DGS. We treat the gray scale as attributes similar to RGB colors for training 3D Gaussians. Similar to representing Gaussian colors using spherical harmonics coefficients, we add identity vectors to 3D Gaussians following

[25, 41]. We set the identity vectors as length 8 to encode segmentation labels ranging from 0 to 255. By conducting differentiable rendering of identity vectors, similar to rendering colors, by blending  $N$  ordered Gaussians on overlapping pixels, we can calculate the identity vectors  $O$  of pixels:

$$O = \sum_{i \in N} o_i \alpha'_i \prod_{j=1}^{i-1} (1 - \alpha'_j) \quad (4)$$

where  $o_i$  represents the identity vector of each Gaussian, and  $\alpha'_i$  is given by evaluating the opacity of 2D Gaussians multiplied by the opacity of each point:

$$\Sigma^{2D} = JW\Sigma^{3D}W^TJ^T \quad (5)$$

where  $\Sigma^{3D}$  is the 3D covariance matrix,  $\Sigma^{2D}$  is the splatted 2D version,  $J$  is the Jacobian matrix for the affine approximation of the 3D to 2D projection, and  $W$  is the world-to-camera transformation matrix. Unlike colors, the identity vectors of the same object does not change with different viewpoints, so we set the SH degree to 0, reducing computational complexity.

**Segment Loss.** Next, we use 3DGS’s 3D consistency to optimize the consistency of segmentation results on the scene images. The L1 loss and SSIM loss in the original 3DGS would lead to the inability to fit object labels. To address this issue, we introduce classification loss and 3D cosine similarity loss. Specifically: 1) For classification loss, we input the rendered identity vectors  $O$  into a linear layer  $f$  followed by a softmax operation:

$$F(O) = \text{softmax}(f(O)) \quad (6)$$

Then we use the standard cross-entropy loss  $L_{oe}$  for classification; 2) For the 3D cosine similarity loss, we sample  $m$  Gaussians, ensuring that the cosine similarity of the identity features  $F_o$  from the  $n$  nearest 3D Gaussians is closely aligned:

$$L_{cs} = \frac{1}{m} \sum_{j=1}^m \text{Cosine Similarity}(A, B) = \frac{1}{mn} \sum_{j=1}^m \sum_{i=1}^n \frac{F(o_j) \cdot F(o_i)}{\|F(o_j)\| \|F(o_i)\|}$$

where set  $A$  contains the identity vectors  $o$  of the sampled 3D Gaussians, and set  $B = o'_1, o'_2, \dots, o'_n$  contains the  $n$  nearest neighbors in 3D space. Making similar 3D Gaussian identity features closer can improve the 3D consistency of segmentation, thus enhancing segmentation accuracy. The total loss function is the weighted sum of the segmentation loss function and the original Gaussian loss function  $L_{gs}$ :

$$L = L_{gs} + \lambda_{oe}L_{oe} + \lambda_{cs}L_{cs} \quad (7)$$

### 3.3 3D Gaussian Extraction and Optimization

After completing scene reconstruction and segmentation, we obtain grouped 3D Gaussians for the entire scene. For 3D Gaussian extraction, we adopt the detected box from Grounding DINO [21] to select the mask ID in a 3D scene. We found that a large complex object may be incorrectly segmented into multiple parts, so our Gaussian extraction supports extracting multiple objects simultaneously and saving them as one object.

**SDS Optimization.** When reconstructing a target within a scene, it often occurs that the target is not fully represented in the original view. This partial representation may be due to a portion of the

target being obscured by other objects, or because of an insufficient range of views. To overcome this, we render images of the object from a variety of random viewpoints and employ SDS loss to optimize the 3DGS model through diffusion priors. Given the target object could be located at arbitrary location within the scene, we ascertain the object’s center by computing the mean value of the 3DGS positions. In the case of objects with differing sizes, we leverage the variance of the 3DGS positions to estimate the size of the object, and accordingly determine the distance between the camera and the object’s center. This approach not only enhances details but also fills in the missing parts of the original view, resulting in a more comprehensive reconstruction.

### 3.4 Mesh Extraction

For mesh extraction, we use SuGaR for further 3DGS optimization and obtaining high-quality object meshes. In order to adapt to SuGaR, we need to obtain view images that contain only the target. Our algorithm goes through two processes to obtain the image. First of all, we render the 3DGS segmentation result of the scene to the original image to obtain the accurate target segmentation result on the original image and erase the background, which forms the first part of the image fed to SuGaR. In addition, since the original scene image does not contain the occluded part or the unseen part of the target, this will cause the missing of views, and the quality of the final mesh will be reduced. To solve this problem, we render images of the SDS-optimized 3DGS from random viewpoints, and supplement the images along with their corresponding camera poses into the input parts of SuGaR. Finally, we input the 3DGS model of the target and the pictures of the two parts into the SuGaR model together to obtain the final target mesh.

## 4 EXPERIMENTS

### 4.1 Implementation Details

All experiments are performed and measured on a single GPU NVIDIA RTX 3090 with Ubuntu 18.04 LTS.

**Datasets** To evaluate the reconstruction quality, we tested our OMEGAS on scenes presented in LERF-MASK dataset[41] and Mip-Nerf360[2], where the flowers and treehill are skipped due to the non-public access right. We also take diverse 3D scene cases from LERF[16], Tanks&Temples[19] and Instruct-NeRF2NeRF[12] for visual comparison.

In 3DGS segmentation, the input to the classification layer has 8 channels, outputting 256. In training,  $\lambda_{oe} = 1.0$  and  $\lambda_{cs} = 2.0$ . We use the Adam[17] optimizer for both Gaussians and linear and train for 7000 iterations with a learning rate of 0.0025 for identity vectors and 0.0005 for linear layer. For 3D regularization loss, we choose  $n = 5$  and  $m = 1000$ .

In 3DGS extraction, we use the GroundingDINO Swin-B model[21] and SAM-HQ model[14]. The probability threshold  $p_{ex}$  for extraction is 0.95.

In SDS optimization, we use the Stable Diffusion 2.1 model[28] and set the resolution to 512. We establish the distance between the camera and the object’s center to be the sum of the object’s size and an additional distance. We set the this distance to 3.0 and the azimuth in  $(-180, 180)$  degree and elevation in  $(-30, 30)$  degree.

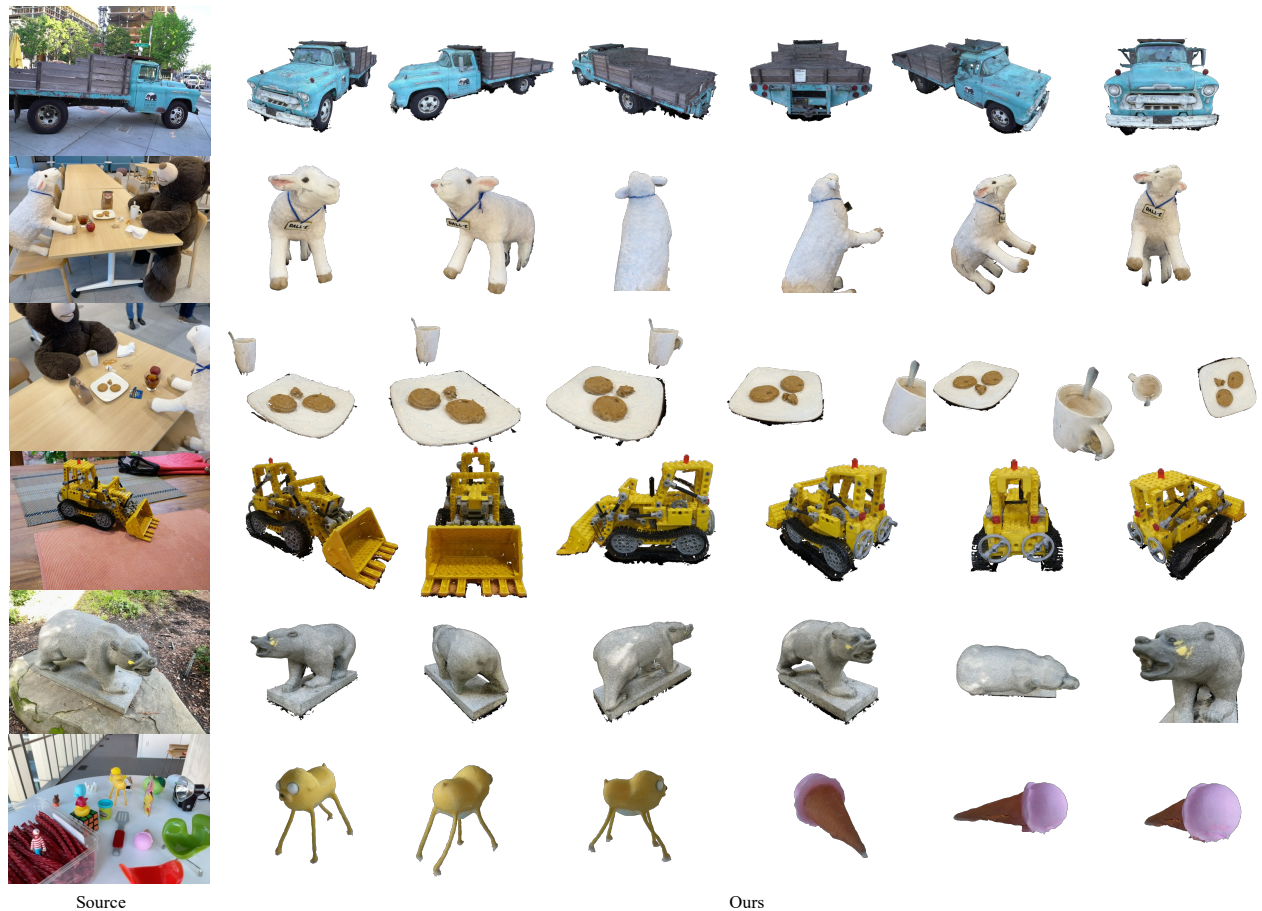


Figure 5: Results of meshes with OMEGAS.

**Table 1: Comparison of segmentation on LERF-MASK dataset[41]. We adopt mIoU and boundary metrics mBIOU for better segmentation quality measurement. The empirical evidence substantiates that our methodology yields superior outcomes in both quality and efficiency.**

Model	figurines			ramen			teatime		
	mIoU $\uparrow$	mBIOU $\uparrow$	time $\downarrow$	mIoU $\uparrow$	mBIOU $\uparrow$	time $\downarrow$	mIoU $\uparrow$	mBIOU $\uparrow$	time $\downarrow$
Gaussian Grouping [41]	86.08	84.08	7min8s	70.34	58.03	6min25s	75.98	71.91	6min54s
<b>Ours</b>	<b>86.21</b>	<b>84.09</b>	<b>6min 11s</b>	<b>86.48</b>	<b>73.62</b>	<b>5min 42s</b>	<b>78.81</b>	<b>73.32</b>	<b>6min 11s</b>

The learning rate for position is decayed from 0.00016 to 0.000016 in 400 steps. The field of view is 30 degree.

In mesh extraction, we set the number of randomly rendered images to 100, and adjust the camera parameters and resolution to match the scene dataset.

## 4.2 Comparative Analysis

**Segmentation Quality and Efficiency** We show the visual segmentation comparison between different vector lengths and loss functions in Figure 4. The experimental results indicate that our method is capable of achieving multi-object segmentation in complex scenes, while simultaneously enhancing the accuracy of the segmentation.

In Table 1, we compare the quality and efficiency of scene segmentation with Gaussian Grouping[41] on LERF-MASK dataset[41]. Owing to the substantial VRAM requirements of Gaussian grouping, completing 7,000 iterations proved unfeasible. For fair comparison, we adjusted our approach to train for an equivalent 5,000 iterations. Within the contexts of the ramen and teatime scenarios, our methodology exhibits a markedly superior segmentation precision compared to GaussianGrouping, while maintaining parity in the figurines scenario. Across all three scenarios, our methodology outpaces GaussianGrouping in terms of training speed, registering an average enhancement of 11.6%. Our method improve segmentation accuracy while reducing time and VRAM using of training.

**Mesh Quality** We provide qualitative comparisons with SuGar[11] and DreamGaussian[32] in Figure 6. We use the teatime, bear and



Figure 6: Comparing mesh extracting results with DreamGaussian[32] and SuGaR[11]. Our method can achieve better object textures and shapes. In addition, our method can directly obtain meshes of the desired objects, reducing the labor of manually selecting object edges and mesh editing.

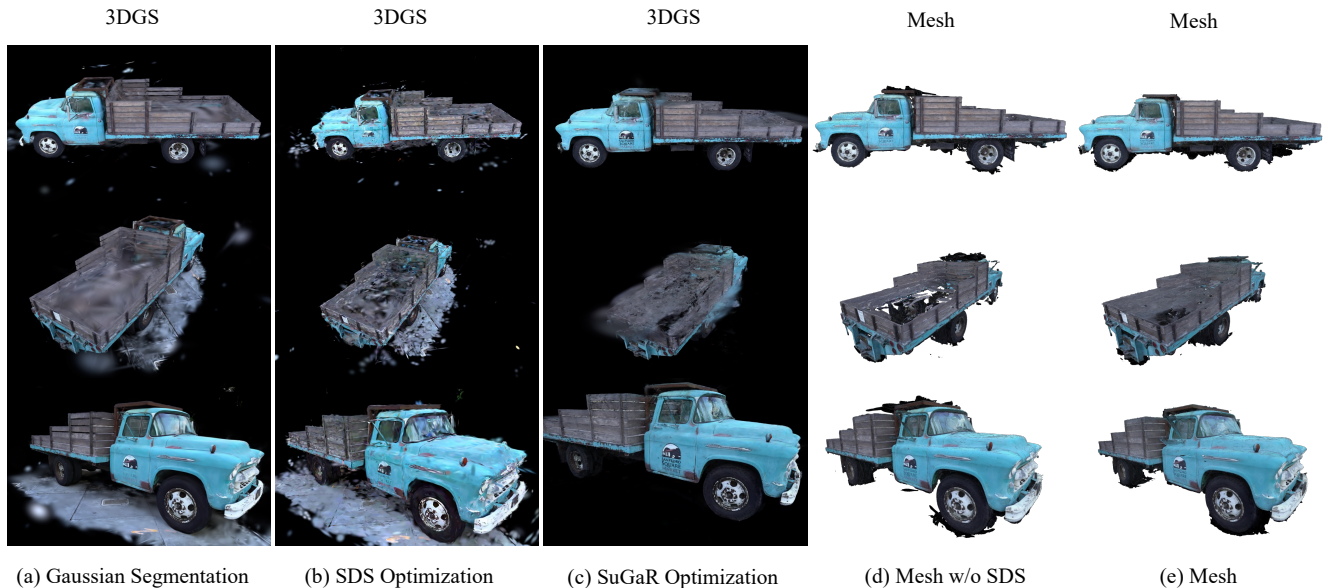


**Figure 7: Ablation study.** We ablate SDS operation on the truck scene from Tanks&Temples dataset[19]. We derive the mesh without SDS by refraining from executing SDS optimization on the 3DGS of the object and abstaining from feeding the random viewpoint image into SuGaR.

kitchen open-world scenes from LERF[16] and Instruct-NeRF2NeRF dataset[12] to compare the quality of the generated mesh. Both SuGaR and our approach utilize multi-view images as input, whereas DreamGaussian employs a single-view image.

In comparison to SuGaR, our method can achieve better details in all three scenes. The attention that SuGaR devotes to the entirety of the scene results in a noticeable reduction in the granularity of local details. Concurrently, our method’s ability to reconstruct unseen portions in the input view is demonstrated in the bear scene. The kitchen scene, on the other hand, showcases the precision of our method in segmenting and extracting complex objects.

Relative to DreamGaussian, our method significantly enhances the quality of the generated meshes.

In Figure 5, we further demonstrate the quality of the mesh and our method’s proficiency in extracting small objects within complex scenes.

### 4.3 Ablation Study

We carry out ablation studies on the design of our methods in Figure 7. We are mainly interested in how SDS optimization affects the Gaussians and mesh of an object, given that mesh optimization has been well explored in previous work[11]. We perform ablation from two perspectives: the occluded and non-occluded parts of the object. We visualize the 3DGS of the object obtained after Gaussian segmentation, SDS optimization, and SuGaR optimization respectively. Additionally, we compare the object mesh that is obtained with and without the process of SDS optimization.

In the case of occluded sections, a comparison between Figure (a) and Figure (b) reveals that SDS optimization enhances the count

of Gaussians in these occluded areas, thereby facilitating the generation of mesh in these regions by SuGaR. A comparison between Figure (d) and Figure (e) indicates a significant reduction in the absence of occluded sections of the object.

In the context of non-occluded sections, a comparison between Figure (a) and Figure (b) demonstrates that SDS optimization exerts both positive and negative impacts on the object. However, a comparison between Figure (b) and Figure (c) reveals that SuGaR is capable of mitigating the negative implications of SDS, thereby culminating in an overall enhancement in the quality of the object.

Furthermore, Figure 6 allows for an ablation of both Gaussian segmentation and SDS optimization. Comparing the use of SuGaR optimization alone with our complete method, it reveals that SuGaR optimization leads to the absence of mesh in the occluded sections of the object.

## 5 CONCLUSION

In conclusion, we introduce OMEGAS: Object Mesh Extraction from Large Scenes Guided by Gaussian Segmentation. This framework effectively extracts high-precision meshes of target objects from multi-view scene images and is capable of reconstructing occluded or otherwise invisible parts of the targets. OMEGAS ingeniously brings together several excellent approaches, including SAM, 3DGS, Stabled Diffusion, and SuGaR model. Compared to baselines, our method shows great superiority to both the detailed texture of the target and the robustness to occlusion. We hope that OMEGAS will give a slight boost to the field of 3D reconstruction and might provide a better solution for downstream tasks.

## 6 APPENDIX

In this supplementary material, we first conduct additional implementation details on gaussian segmentation in Sec 6.1. Then, in Sec 6.2, we describe the detailed process on gaussian extraction. We further provide additional details on the generation of meshes using SuGaR in Sec 6.3. In Section 6.4, we provide additional details regarding the evaluation experiments presented in our comparative analysis. The visual results of the Gaussian extraction phase are vividly displayed in Sec 6.5. Finally, in Section 6.6, we furnish supplementary results of our ablation studies.

### 6.1 More details on Gaussian Segmentation

We start the densification process from the 500th iteration, with a densification interval set to 100. The interval for resetting opacity is set to 3000. Every 5 iterations, we use the sum of the segmentation loss and gaussian loss as the loss function, while for the rest, we only use the gaussian loss.

### 6.2 More details on Gaussian Extraction

For 3D Gaussian extraction, we adopt Grounding DINO [21] and SAM[14] to segment a scene image, obtaining a mask corresponding to the text prompt. We select the IDs within the mask area that exceed a threshold of  $p_{id}$  as the IDs for the corresponding objects. Subsequently, we utilize a classifier to obtain the category probabilities for each Gaussian. We then select the Gaussians that have a probability greater than  $p_{ex}$  for belonging to this ID, as well as the Gaussians that are encompassed within its convex hull, for extraction and preservation. As mentioned in implementation details of our paper, the threshold  $p_{ex}$  for extracting Gaussians is set to 0.95. Meanwhile, the threshold  $p_{id}$  for extraction is 0.5.

### 6.3 Implementation details on SuGaR

While employing SuGaR for the extraction of mesh, we fundamentally conform to the parameter configurations prescribed by SuGaR[11].

In the regularization step, the optimization process begins with a Gaussian Splatting that has no regularization, which is carried out for 7,000 iterations. This is followed by 2,000 iterations that include an additional entropy loss on the opacities of the Gaussians, serving as a method to enforce binary values. Subsequently, Gaussians with opacity values below 0.5 are removed, and 6,000 iterations are performed with the regularization term. This brings the total to 15,000 iterations. The sum of the Gaussian functions from the 16 nearest Gaussians is computed, and the list of nearest neighbors is updated every 500 iterations. The optimization process typically takes between 15 and 45 minutes, depending on the scene. In the mesh extraction step, the set of the density function is extracted for  $\lambda = 0.3$ . Poisson reconstruction is performed with a depth of 10, and mesh simplification is applied using quadric error metrics to reduce the resolution of the meshes. The mesh extraction process generally takes between 5 and 10 minutes, depending on the scene. During the joint refinement, the mesh and the bound 3D Gaussians are refined jointly for either 2,000, 7,000, or 15,000 iterations. For smaller objects, we perform 7000 iterations. The duration of the refinement process ranges from a few minutes to an hour, depending on the number of iterations.

### 6.4 More details on evaluation

We provide additional details regarding the evaluation experiments presented in our comparative analysis. To measure the segmentation or fine-grained localization accuracy in open-wold 3D scene, we use the LERF-Mask dataset[41] based on the LERF-Localization evaluation dataset[16]. For each 3D scene, we use 6 text queries with corresponding GT mask label in average. Similar to the annotation used in LERF[16], for each of the 3 scenes, we choose 2-4 novel views for testing and annotating the rendering of novel views. All language prompts used for LERF-Mask dataset evaluation are listed in Table 2, which contains 18 prompts in total.

Scene	Text queries	
Figurines	green apple	green toy chair
	old camera	porcelain hand
	red toy chair	rubber duck with red hat
Ramen	chopsticks	egg
	pork belly	yellow bowl
Teatime	bag of cookies	cookies on a plate
	sheep	apple
	paper napkin	coffee mug
	bear	tea in a glass

**Table 2: Prompt labels used during segmentation experiments in LERF-Mask dataset[41].**

### 6.5 Additional Results for Gaussian Extraction

We provide visualization on the gaussian extraction in Figure 8. We use three scenes from the LERF dataset[16], each scene being input with an object prompt. Through Gaussian extraction, we obtain the ID and 3DGS of the corresponding object. Our presentation encompasses the images rendered from each scene, the segmentation outcomes derived from the utilization of Grounding DINO[21] and SAM[14], along with the masks rendered from the 3DGS of the extracted objects.

### 6.6 Additional Results for Ablation Study

We carry out additional ablation studies in figure 9 on the ‘bear’ scene from the Instruct-NeRF2NeRF dataset[12]. The outcomes further elucidate the proficiency of SDS optimization in the reconstruction of the occluded areas.

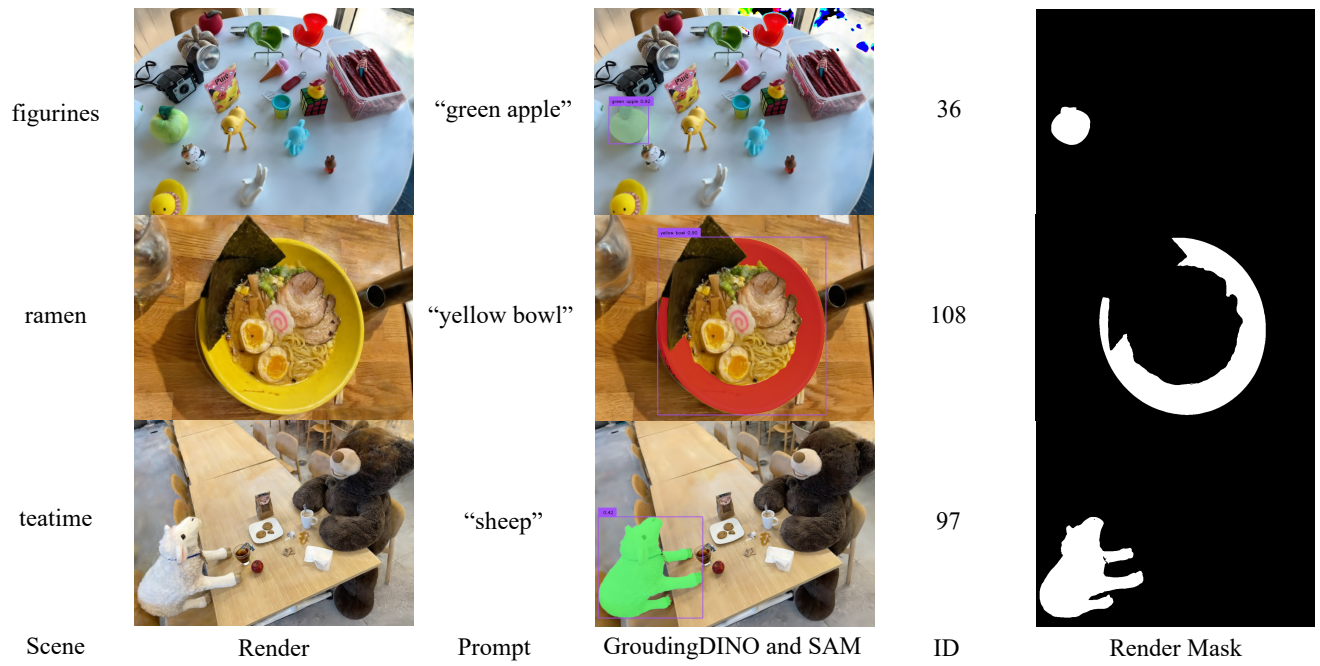


Figure 8: Visualization of the gaussian extraction

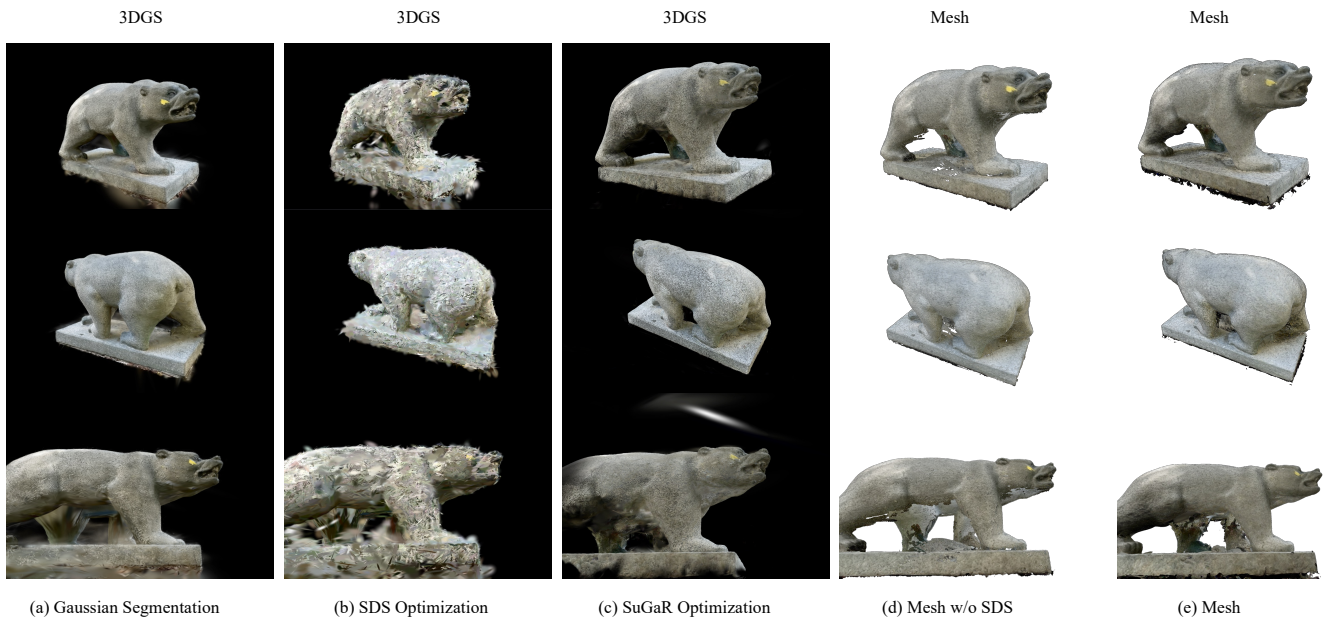


Figure 9: Additional ablation study in the ‘bear’ scene from the Instruct-NeRF2NeRF dataset[12].

## REFERENCES

- [1] Jonathan T Barron, Ben Mildenhall, Matthew Tancik, Peter Hedman, Ricardo Martin-Brualla, and Pratul P Srinivasan. 2021. Mip-nerf: A multiscale representation for anti-aliasing neural radiance fields. In *Proceedings of the IEEE/CVF International Conference on Computer Vision*. 5855–5864.
- [2] Jonathan T Barron, Ben Mildenhall, Dor Verbin, Pratul P Srinivasan, and Peter Hedman. 2022. Mip-nerf 360: Unbounded anti-aliased neural radiance fields. In *Proceedings of the IEEE/CVF Conference on Computer Vision and Pattern Recognition*. 5470–5479.
- [3] Inês Caetano, Luis Santos, and António Leitão. 2020. Computational design in architecture: Defining parametric, generative, and algorithmic design. *Frontiers of Architectural Research* 9, 2 (2020), 287–300.
- [4] Pu Cao, Lu Yang, Feng Zhou, Tianrui Huang, and Qing Song. 2023. Concept-centric Personalization with Large-scale Diffusion Priors. *ArXiv abs/2312.08195* (2023). <https://api.semanticscholar.org/CorpusID:266191061>
- [5] Pu Cao, Feng Zhou, Qing Song, and Lu Yang. 2024. Controllable Generation with Text-to-Image Diffusion Models: A Survey. *ArXiv abs/2403.04279* (2024). <https://api.semanticscholar.org/CorpusID:268264822>
- [6] Jiazhong Cen, Zanwei Zhou, Jiemin Fang, Chen Yang, Wei Shen, Lingxi Xie, Xiaopeng Zhang, and Qi Tian. 2023. Segment Anything in 3D with NeRFs. In *NeurIPS*.
- [7] Ho Kei Cheng, Seoung Wug Oh, Brian Price, Alexander Schwing, and Joon-Young Lee. 2023. Tracking anything with decoupled video segmentation. In *Proceedings of the IEEE/CVF International Conference on Computer Vision*. 1316–1326.
- [8] François Darmon, Bénédicte Bascle, Jean-Clément Devaux, Pascal Monasse, and Mathieu Aubry. 2022. Improving neural implicit surfaces geometry with patch warping. In *Proceedings of the IEEE/CVF Conference on Computer Vision and Pattern Recognition*. 6260–6269.
- [9] Siqi Fan, Qiulei Dong, Fenghua Zhu, Yisheng Lv, Peijun Ye, and Fei-Yue Wang. 2021. SCF-Net: Learning spatial contextual features for large-scale point cloud segmentation. In *Proceedings of the IEEE/CVF Conference on Computer Vision and Pattern Recognition*. 14504–14513.
- [10] Michael Goesele, Noah Snavely, Brian Curless, Hugues Hoppe, and Steven M Seitz. 2007. Multi-view stereo for community photo collections. In *2007 IEEE 11th International Conference on Computer Vision*. IEEE, 1–8.
- [11] Antoine Guédon and Vincent Lepetit. 2023. SuGaR: Surface-Aligned Gaussian Splatting for Efficient 3D Mesh Reconstruction and High-Quality Mesh Rendering. *ArXiv abs/2311.12775* (2023). <https://api.semanticscholar.org/CorpusID:265308825>
- [12] Ayaan Haque, Matthew Tancik, Alexei Efros, Aleksander Holynski, and Angjoo Kanazawa. 2023. Instruct-NeRF2NeRF: Editing 3D Scenes with Instructions. In *ICCV*.
- [13] Michael Kazhdan, Matthew Bolitho, and Hugues Hoppe. 2006. Poisson surface reconstruction. In *Proceedings of the fourth Eurographics symposium on Geometry processing*, Vol. 7.
- [14] Lei Ke, Mingqiao Ye, Martin Danelljan, Yifan Liu, Yu-Wing Tai, Chi-Keung Tang, and Fisher Yu. 2023. Segment Anything in High Quality. In *NeurIPS*.
- [15] Bernhard Kerbl, Georgios Kopanas, Thomas Leimkühler, and George Drettakis. 2023. 3d gaussian splatting for real-time radiance field rendering. *ACM Transactions on Graphics* 42, 4 (2023), 1–14.
- [16] Justin Kerr, Chung Min Kim, Ken Goldberg, Angjoo Kanazawa, and Matthew Tancik. 2023. LERF: Language Embedded Radiance Fields. In *ICCV*.
- [17] Diederik P. Kingma and Jimmy Ba. 2014. Adam: A Method for Stochastic Optimization. *CoRR abs/1412.6980* (2014). <https://api.semanticscholar.org/CorpusID:6628106>
- [18] Alexander Kirillov, Eric Mintun, Nikhila Ravi, Hanzi Mao, Chloe Rolland, Laura Gustafson, Tete Xiao, Spencer Whitehead, Alexander C Berg, Wan-Yen Lo, et al. 2023. Segment anything. In *ICCV*.
- [19] Arno Knapitsch, Jaesik Park, Qian-Yi Zhou, and Vladlen Koltun. 2017. Tanks and temples: Benchmarking large-scale scene reconstruction. *ACM Transactions on Graphics (ToG)* 36, 4 (2017), 1–13.
- [20] Zhaoshuo Li, Thomas Müller, Alex Evans, Russell H Taylor, Mathias Unberath, Ming-Yu Liu, and Chen-Hsuan Lin. 2023. Neuralangelo: High-fidelity neural surface reconstruction. In *Proceedings of the IEEE/CVF Conference on Computer Vision and Pattern Recognition*. 8456–8465.
- [21] Shilong Liu, Zhaoyang Zeng, Tianhe Ren, Feng Li, Hao Zhang, Jie Yang, Chunyuan Li, Jianwei Yang, Hang Su, Jun Zhu, et al. 2023. Grounding dino: Marrying dino with grounded pre-training for open-set object detection. *arXiv preprint arXiv:2303.05499* (2023).
- [22] Xian Liu, Xiaohang Zhan, Jiayang Tang, Ying Shan, Gang Zeng, Dahua Lin, Xihui Liu, and Ziwei Liu. 2023. Humangaussian: Text-driven 3d human generation with gaussian splatting. *arXiv preprint arXiv:2311.17061* (2023).
- [23] William E. Lorensen and Harvey E. Cline. 1987. Marching cubes: A high resolution 3D surface construction algorithm. *Proceedings of the 14th annual conference on Computer graphics and interactive techniques* (1987). <https://api.semanticscholar.org/CorpusID:15545924>
- [24] Ben Mildenhall, Pratul P. Srinivasan, Matthew Tancik, Jonathan T. Barron, Ravi Ramamoorthi, and Ren Ng. 2020. NeRF: Representing Scenes as Neural Radiance Fields for View Synthesis. In *ECCV*.
- [25] Ashkan Mirzaei, Tristan Aumentado-Armstrong, Konstantinos G Derpanis, Jonathan Kelly, Marcus A Brubaker, Igor Gilitschenski, and Alex Levinshstein. 2023. SPIn-NeRF: Multiview segmentation and perceptual inpainting with neural radiance fields. In *CVPR*.
- [26] Michael Oechsle, Songyou Peng, and Andreas Geiger. 2021. Unisurf: Unifying neural implicit surfaces and radiance fields for multi-view reconstruction. In *Proceedings of the IEEE/CVF International Conference on Computer Vision*. 5589–5599.
- [27] Ben Poole, Ajay Jain, Jonathan T Barron, and Ben Mildenhall. 2022. Dreamfusion: Text-to-3d using 2d diffusion. *arXiv preprint arXiv:2209.14988* (2022).
- [28] Robin Rombach, Andreas Blattmann, Dominik Lorenz, Patrick Esser, and Björn Ommer. 2022. High-resolution image synthesis with latent diffusion models. In *Proceedings of the IEEE/CVF conference on computer vision and pattern recognition*. 10684–10695.
- [29] Chitwan Saharia, William Chan, Saurabh Saxena, Lala Li, Jay Whang, Emily L Denton, Kamyar Ghasemipour, Raphael Gontijo Lopes, Burcu Karagol Ayan, Tim Salimans, et al. 2022. Photorealistic text-to-image diffusion models with deep language understanding. *Advances in neural information processing systems* 35 (2022), 36479–36494.
- [30] Bruno Siciliano, Oussama Khatib, and Torsten Kröger. 2008. *Springer handbook of robotics*. Vol. 200. Springer.
- [31] Noah Snavely, Steven M Seitz, and Richard Szeliski. 2006. Photo tourism: exploring photo collections in 3D. In *ACM siggraph 2006 papers*. 835–846.
- [32] Jiayang Tang, Jiawei Ren, Hang Zhou, Ziwei Liu, and Gang Zeng. 2023. Dreamgaussian: Generative gaussian splatting for efficient 3d content creation. *arXiv preprint arXiv:2309.16653* (2023).
- [33] Haochen Wang, Xiaodan Du, Jiahao Li, Raymond A Yeh, and Greg Shakhnarovich. 2023. Score jacobian chaining: Lifting pretrained 2d diffusion models for 3d generation. In *Proceedings of the IEEE/CVF Conference on Computer Vision and Pattern Recognition*. 12619–12629.
- [34] Peng Wang, Lingjie Liu, Yuan Liu, Christian Theobalt, Taku Komura, and Wenping Wang. 2021. Neus: Learning neural implicit surfaces by volume rendering for multi-view reconstruction. *arXiv preprint arXiv:2106.10689* (2021).
- [35] Zhengyi Wang, Cheng Lu, Yikai Wang, Fan Bao, Chongxuan Li, Hang Su, and Jun Zhu. 2024. Prolificdreamer: High-fidelity and diverse text-to-3d generation with variational score distillation. *Advances in Neural Information Processing Systems* 36 (2024).
- [36] Guanjun Wu, Taoran Yi, Jiemin Fang, Lingxi Xie, Xiaopeng Zhang, Wei Wei, Wenyu Liu, Qi Tian, and Xinggang Wang. 2023. 4d gaussian splatting for real-time dynamic scene rendering. *arXiv preprint arXiv:2310.08528* (2023).
- [37] Jianghao Xiong, En-Lin Hsiang, Ziqian He, Tao Zhan, and Shin-Tson Wu. 2021. Augmented reality and virtual reality displays: emerging technologies and future perspectives. *Light: Science & Applications* 10, 1 (2021), 1–30.
- [38] Chenfeng Xu, Bichen Wu, Zining Wang, Wei Zhan, Peter Vajda, Kurt Keutzer, and Masayoshi Tomizuka. 2020. SqueezeSegv3: Spatially-adaptive convolution for efficient point-cloud segmentation. In *Computer Vision—ECCV 2020: 16th European Conference, Glasgow, UK, August 23–28, 2020, Proceedings, Part XXVIII* 16. Springer, 1–19.
- [39] Bangbang Yang, Chong Bao, Junyi Zeng, Hujun Bao, Yinda Zhang, Zhaopeng Cui, and Guofeng Zhang. 2022. Neumesh: Learning disentangled neural mesh-based implicit field for geometry and texture editing. In *European Conference on Computer Vision*. Springer, 597–614.
- [40] Ziyi Yang, Xinyu Gao, Wen Zhou, Shaohui Jiao, Yuqing Zhang, and Xiaogang Jin. 2023. Deformable 3d gaussians for high-fidelity monocular dynamic scene reconstruction. *arXiv preprint arXiv:2309.13101* (2023).
- [41] Mingqiao Ye, Martin Danelljan, Fisher Yu, and Lei Ke. 2023. Gaussian Grouping: Segment and Edit Anything in 3D Scenes. *ArXiv abs/2312.00732* (2023). <https://api.semanticscholar.org/CorpusID:265551523>
- [42] Taoran Yi, Jiemin Fang, Guanjun Wu, Lingxi Xie, Xiaopeng Zhang, Wenyu Liu, Qi Tian, and Xinggang Wang. 2023. Gaussiandreamer: Fast generation from text to 3d gaussian splatting with point cloud priors. *arXiv preprint arXiv:2310.08529* (2023).
- [43] Alex Yu, Vickie Ye, Matthew Tancik, and Angjoo Kanazawa. 2021. pixelnerf: Neural radiance fields from one or few images. In *Proceedings of the IEEE/CVF Conference on Computer Vision and Pattern Recognition*. 4578–4587.